

**Liquid-to-solid transition of concentrated suspensions under complex transient shear histories**Ying Guo,<sup>1</sup> Wei Yu,<sup>1,\*</sup> Yuanze Xu,<sup>2</sup> and Chixing Zhou<sup>1</sup><sup>1</sup>*Advanced Rheology Institute, Department of Polymer Science and Engineering, Shanghai Jiao Tong University, Shanghai 200240, People's Republic of China*<sup>2</sup>*The Key Laboratory of Molecular Engineering of Polymers, Ministry of Education, Department of Macromolecular Science, Fudan University, Shanghai 200433, People's Republic of China*

(Received 11 August 2009; revised manuscript received 19 October 2009; published 15 December 2009)

Suspensions containing noncolloidal aluminum particles in a Newtonian carrier liquid and the effects of shear history on the rheological properties of suspensions are investigated showing a critical concentration  $\phi_c$ , which is close to the “freezing” packing fraction of spherical particle suspensions. An apparent liquid-to-solid transition was clearly found for suspensions below  $\phi_c$  via transient step shear after long shear history as well as via the large amplitude oscillatory shear flow with controlled shear stress. The microstructures or the local flow characteristics of suspensions with  $\phi < \phi_c$  and with  $\phi > \phi_c$  are still different according to the Fourier Transform Rheological analysis. Although suspensions with  $\phi < \phi_c$  show solidlike behaviors after long shear history, the flow behaviors keep unchanged as shear stress increases, and typically show solidlike, liquid-solid coexistence, liquidlike, and jamming behaviors, successively. However, liquidlike regime of concentrated suspensions with  $\phi > \phi_c$  disappears after preshear.

DOI: [10.1103/PhysRevE.80.061404](https://doi.org/10.1103/PhysRevE.80.061404)

PACS number(s): 83.80.Hj

**I. INTRODUCTION**

The rheology of concentrated suspensions and slurries has attracted much interest in recent years due to its obvious importance in a wide range of industrial applications, including inkjet printing, coating, and energetic materials as well as civil engineering applications. The highly concentrated suspensions behave much higher complexity than the present suspension rheology predicts. The filling degree of solid ingredients is maximized for many applications to be as close as possible to the maximum packing fraction. The maximum packing fraction itself is increased to very high values by the tailoring of the particle shape and the size distributions of the solid ingredients, as well as controlling the particle interactions. The complex rheological properties of highly concentrated suspensions are strongly affected by the change in the microstructure in various deformation histories. Some rheological and rheo-optical methods [1,2] have been used to understand the change in the suspension microstructure under various flows by transient experiments [3–8], Fourier-transform rheology [5,8,9], as well as the virtual experimental simulations [10,11]

The most important and controversial property of the high concentrated suspensions is the yield stress, which causes suspensions to behave as viscoplastic fluids and display plastic behavior at low shear stress and viscous behavior at high shear stress. Yielding corresponds to the transition from solidlike state (“frozen equilibrium”) to liquidlike state, associated with breakup of the initial particle configuration, such as particle network of direct contacts. Heymann and co-workers studied the solid-liquid transition of suspensions using transient and oscillatory shear under Controlled-Shear-Rates (CSR) and Controlled-Shear-Stress (CSS) mode [4–6]. The

behavior under different flow type [5,9] provided evidence that this transition is a highly nonlinear and complex process, which show the simultaneous dependences of the shear stress on the shear strain, shear rate, and ramp time. Suspension instability caused by the collapse of the particle network structure is usually regarded as the origin of this transition behavior. Nevertheless, these investigations on the transition behavior were limited to the comparison of two types of mechanical histories, i.e., the steady preshear and the oscillatory preshear. It is well-known that concentrated suspensions always display thixotropic properties, and it is still unclear about the nature of shearing time or shear intensity on the transition behavior up to now.

On the other hand, the complexity of suspension rheology also shows that the macroscopic flow behaviors of concentrated suspensions are not equal to its microscopic properties or local rheology, i.e., the suspension can have a different microscopic transition from the apparent one. Coussot and co-workers [12–14] studied the local velocity and concentration profile of concentrated suspensions in Couette flow through magnetic resonance imaging (MRI) technique. They found suspensions developed evident transition from severe heterogeneous state to homogeneous state as the applied velocity or stress increased. This transition behavior can be attributed to structural changes in particle network.

To probe the structures of microstructures, oscillatory shear flow is known to be a good choice. However, the linear viscoelasticity under small amplitude oscillatory shear has been found to be insufficient due to readily appearance of nonlinear behavior. The harmonic analysis through Fourier-transform rheology (FTR) provides an alternative to detect the structure change in particle network. As the amplitude of the input sinusoidal signal increases, exceeding the critical value for the linear region, the output signal in most cases is periodic and contains higher harmonics [15]. In the nonlinear region, the occurrence of odd frequency components is often used to study structural changes or modifications [16–18], and also as an indication of fluid inertia [15,19] The appear-

---

\*Author to whom all correspondence should be addressed; [wyu@sjtu.edu.cn](mailto:wyu@sjtu.edu.cn)

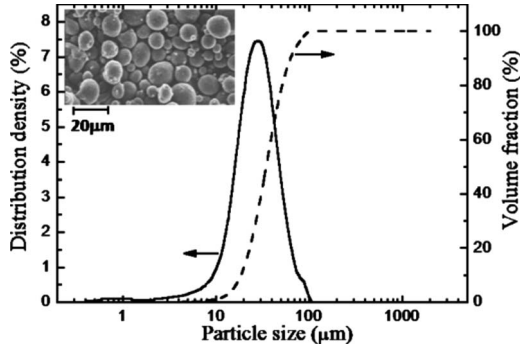


FIG. 1. Size distribution of the aluminum particles. Inset: SEM image of the particles.

ance of even harmonics with high intensity always occurs in the concentrated suspensions, and wall slip [20,21] is supposed to be the main reason for the occurrence of even harmonics. Other possible reasons for the occurrence of even harmonics are the experimental insufficiencies [18,22] and the yield stress [22,23]. Considering the connection between the structures of suspension and the nonlinear rheological behaviors, it is reasonable to describe the microscopic transition in large amplitude oscillatory shear (LAOS) flow with different preshear histories by the method of FTR.

In this work, we will elucidate two types of preshear conditions used in the experiments as described in Sec. II B. We present the results of transient normalized stress response as a function of the strain in Sec. III B, and normalized oscillatory stress using strain of fundamental frequency and the third harmonic strain, respectively, in Sec. III C. Then we use the critical stress as the key parameter to analyze the effects of shear history on suspension microstructure under the nonlinear oscillatory shear flow (Sec. III D). Finally, we give the conclusions in Sec. IV.

## II. EXPERIMENT

### A. Formulation and preparation

The investigated suspensions consist of aluminum powder dispersed in a low viscosity ( $\eta_m$ ) Newtonian matrix. The matrix is a mixture of hydroxyl-terminated ethylene oxide-tetrahydrofuran copolymer (PET,  $M_n=3810$  g/mol, 28.6wt%, Fourth Academy of China Aerospace Science and Technology Corporation) and glycerol diacetate (GDA, 71.4wt%, Yixing Tianyuan Chemical Co., Ltd.). The matrix exhibits Newtonian behavior under all the shear conditions studied here with the viscosity  $\eta_m=2.7$  Pa·s at 30 °C. The density of the matrix is  $\rho_m=1230$  kg/m<sup>3</sup> at 30 °C. The solid phase is spherical aluminum particles (Fourth Academy of China Aerospace Science and Technology Corporation) with narrow size distribution and the volume average diameter  $d_p=45.3$  μm, measured with a LS230 laser particle size analyzer (Beckman Coulter, USA), as shown in Fig. 1. The density of the aluminum particles is  $\rho_p=2700$  kg/m<sup>3</sup>. A scanning electronic microscopy (SEM) image of the aluminum powder is shown in the inset of Fig. 1.

The maximum particle-based Reynolds number for the systems used is low ( $R_{ep}=d_p v \rho_p / \eta_m \approx 10^{-4}$ , where the maxi-

um shear rate  $\dot{\gamma}$  is about 5 s<sup>-1</sup> and the corresponding particle velocity  $v$  is about 8 mm/s.) and the Péclet number is very high ( $Pe=6\pi\eta_m\dot{\gamma}r^3/k_B T \approx 10^7$ , where the minimum shear rate  $\dot{\gamma}$  is about 0.1 s<sup>-1</sup>, and  $r$  is the particle radius, designated by 22.65 μm.). Then, Brownian forces between the particles can be neglected. Consequently, the particle interactions can be considered as of hydrodynamic origin, and the interparticle interactions including granular interactions are likely important as particles become close at high packing fractions. Due to the high matrix-particle density difference, the settling velocity of a single aluminum particle in the matrix was estimated to be about 36 μm/min according to Stokes' law [ $U=d_p^2(\rho_p-\rho_m)g/18\eta_m$ ]. However, the sedimentation will be even slower due to the high volume concentrations. In fact, the settling velocity could be reduced to 1.94 μm/min if the matrix viscosity is replaced by the suspension viscosity (about 50 Pa·s). The settling effect on the rheological measurements is also examined experimentally through stress amplitude sweep. Sweep tests were repeated after four and six hours rest. No dependence has been found on the resting time. The resting time here is much larger than the usual testing time spent during transient or nonlinear oscillatory indicating the settling effects could justifiably be considered negligible during the rheological experiments.

The maximum packing fraction  $\phi_m$  based on the particle size distribution [24] was calculated to be about 64.5vol%, only slightly larger than the random packing fraction for monodispersed spherical suspensions ( $\approx 0.637$ ) [25] due to the relatively narrow particle size distribution. Suspensions with different concentrations, ranged from 40.4 to 57.6 vol%, were prepared. Before preparing the suspensions, the particles were dried in a vacuum oven for 5 h to remove any residual water. The suspensions were prepared in two steps. At first, the homogeneous matrix was obtained by magnetic stirring the copolymer and glycerol diacetate (GDA). Then, all suspensions were prepared by mechanical mixing the particles in small increments until a homogeneous state was reached. The suspensions were mechanical stirred in 30 min at speed of 100 rpm. The air incorporated during mixing was removed by letting the sample rest for 2 h.

### B. Equipment and methods

Experiments were performed using a stress-controlled rotational rheometer (Bohlin Gemini 200HR, Malvern Instruments Ltd.) equipped with a Couette geometry. The Couette geometry consisted of a rotating bob with radius  $R_i=17.5$  mm, a stationary cup with radius  $R_o=19.2$  mm, and the bob height was 17.81 mm with gap  $d=1.7$  mm. All the measurements were conducted at the temperature of 30 °C. The following are the details of the individual tests performed.

First, the effects of preshear on the rheology of suspensions are investigated with three elementary procedures: SR1, SR2, and SR3, as illustrated in

Figure 2 SR1 consists of shearing the materials with  $\dot{\gamma}_0$  (0.1 s<sup>-1</sup>, 0.5 s<sup>-1</sup>, 1 s<sup>-1</sup>, and 5 s<sup>-1</sup>) for a period  $t_0$  followed by a resting time  $t_0$ , and then the shearing was immediately applied in the same direction with constant shear rate  $\dot{\gamma}_a$

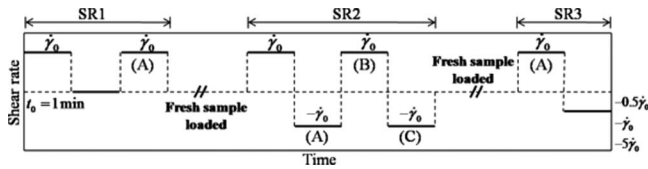


FIG. 2. Schematic diagram of short shear history (SSH).

$= \dot{\gamma}_0$  for another period  $t_0$ , and the transient stress responses were recorded. SR2 is designed differing from SR1 in the direction of shear after the first positive shear, where an opposite shear was applied after the first positive shearing, and the magnitude of the shear rate  $\dot{\gamma}_a$  was same as  $\dot{\gamma}_0$ . This process was repeated for one more time. SR3 changed the magnitudes of the reversal shear rate with the value  $\dot{\gamma}_a = -0.5\dot{\gamma}_0, -\dot{\gamma}_0, -5\dot{\gamma}_0$ . All the steps in the three procedures were performed for the same time  $t_0$ . These shear procedures are regarded as short shear history (SSH). The three procedures SR1, SR2, SR3 were also carried out in a series with two rest time intervals to obtain the long shear history (LSH), as showed in Fig. 3.

On the other hand, the large amplitude oscillatory shear was performed immediately after the transient shear to investigate the nonlinear properties and the effects of shear history on the nonlinear behaviors. The LAOS experiments without preshear were also performed as references. During the amplitude sweeps the primary sinusoidal stress signals were applied and the primary signals of the shear strain were measured. The basic frequency of all amplitude sweeps was  $\omega_0 = 6.283$  rad/s. Typically, 20 preliminary oscillations [26] were applied to guarantee the equilibrium state at each measuring value. In order to increase the signal-to-noise ratio (S/N), the data of 4096 points were collected for each period.

### III. RESULTS AND DISCUSSION

#### A. Critical concentration $\phi_c$

With increasing concentrations of noncolloidal solid particles, the distance between particles decreases substantially, and approaches zero as the volume fraction reaches the random packing fraction,  $\phi_m$ . The interparticle interactions (hydrodynamic interaction and contacting forces) are expected to become increasingly important, and the rheological behaviors show distinct changes. Non-Newtonian behavior is generally observed for solids concentrations exceeding 40 vol% [27], and yield stresses have mostly been reported at higher concentrations above 50 vol% [28]. Therefore, it is expected that there exists some critical concentration which is related to the transition behaviors in rheological properties such as yield stress, thixotropy, and shear thickening.

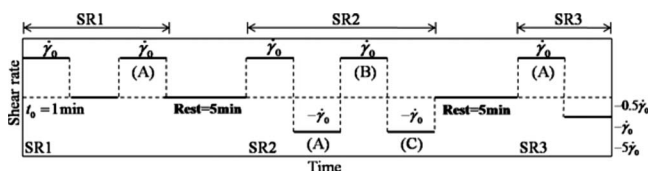


FIG. 3. Schematic diagram of long shear history (LSH).

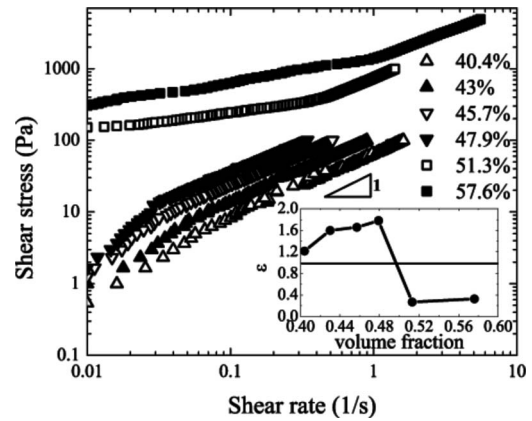


FIG. 4. Shear stress vs shear rate for suspensions. Line: slope 1 indicates Newtonian flow. Inset: inverse slope of thickening region for suspension 40.4%–47.9%.

The yield phenomenon and shear thickening of the suspensions were examined through increasing stress ramps. Shear stress was increased linearly with time from the initial to final shear stress. The ramp time of the time-dependent shear stress was fixed at 300 s. Figure 4 shows shear stress vs shear rate curves for different concentrations. On a log-log plot a slope of unity corresponds to Newtonian flow, a slope between zero and unity indicate shear thinning, while a slope greater than unity means shear thickening. It is shown in Fig. 4 that for suspensions with smaller concentration (40.4% ~ 47.9%) exhibit shear thickening followed by a Newtonian flow behavior, while suspensions with higher concentrations (51.3% ~ 57.6%) show shear thinning before a Newtonian flow behavior. The slope  $\varepsilon$  in these curves ( $\tau \propto \dot{\gamma}^\varepsilon$ ) before the Newtonian flow regime can be used to differentiate the shear thinning ( $\varepsilon < 1$ ) or shear thickening ( $\varepsilon > 1$ ) behavior in different suspensions. The inset of Fig. 4 shows the dependence of slope on volume fraction, which shows a critical concentration  $\phi_c$  about 48~51 vol%. The disappearance of shear thickening behavior is ascribed to the dominating behavior of yield stress in the total shear stress, which result in jamming and shear-thinning behaviors only. Similar behaviors have also been shown in suspensions with almost monodispersed spherical particles and irregular particles [29]. On the other hand, yield stress has also been reported to show similar transitions [29]. However, the yield stress ( $\tau_y$ ) has turned out to be difficult to measure, and it depends on the testing geometry and the detailed experimental protocol. It is seen from Fig. 4 that only suspensions with higher concentration (51.3% ~ 57.6%) show yield like behavior, while almost no yield stress is observed for suspensions with smaller concentration (40.4% ~ 47.9%). Such phenomena also suggest certain transition below 51.3%, but it is difficult to determine the exact transition point from yield stress. This is a little different from the results shown by Brown *et al.* [29], who showed a rapid increase in yield stress when the concentration increases and approaches the critical concentration. This likely can be ascribed to the polydispersity [3,30,31] of the particle size and density mismatch [32] in our system. However, it is hard to say which one is the most important factor. First, suspensions of noncolloidal particles with narrow size

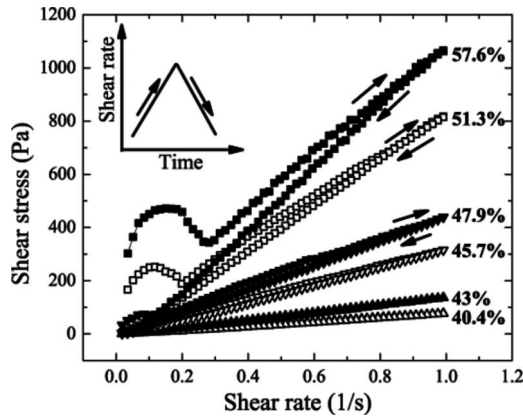


FIG. 5. Evolution of shear stress with shear rate for suspensions. Inset: procedure of shear rate ramp.

distributions display shear-thinning behavior observed by various experimental techniques [3,30,31]. Shear thinning was detected at  $\phi=40\%$ , and the amount of shear thinning increased as the concentration increased. The non-Newtonian behavior in suspensions with narrow size distribution was different from the bimodal suspensions or suspensions of large particles. In falling-ball experiments, Reardon and co-workers [31] show that suspensions below 30% have relative viscosity that is independent of size distribution. At high concentrations up to 50%, suspensions display size distribution dependent viscosity and becomes more shear thinning. In these experiments, it is clear to see that the yield behavior is greatly affected by the polydispersity of particles since the shear-thinning is strongly linked with the yield stress. On the other hand, the competition between gravity and viscous stresses plays an important role in the development of a yield stress in concentrated suspensions [32]. The authors showed that the yield stress can actually be ascribed completely to the frictional behavior of the granular matrix under normal stresses due to the difference of density. The difference of density between particle and fluid in our system is about  $1470 \text{ kg/m}^3$ , while the density mismatch was assumed to be negligible for glass beads and chose as zero for starch particles in Brown *et al.* [29].

The thixotropy of suspensions was also investigated, and the shear rate ramp was started from  $0.01$  to  $1 \text{ s}^{-1}$  within the rise up time  $360 \text{ s}$ , then ramp down to  $0.01 \text{ s}^{-1}$  within the same time period, see the inset of Fig. 5. The area of the thixotropic loop was used to characterize the thixotropy of the suspensions, i.e., larger loop area indicates stronger thixotropy, see Fig. 7(c). Below the critical concentration  $\phi_c$ , suspensions exhibits a very small yield stress and weak thixotropy, while large yield stress and strong thixotropy are shown for concentrations higher than  $\phi_c$ , as shown in Fig. 5. The yield stress above  $\phi_c$  has a great contribution on the area of the thixotropic loop [4].

Compared with the transient shear flow mentioned above, oscillatory shear was also used to study the critical fraction. The amplitude sweeps at a frequency of  $\omega=6.283 \text{ rad/s}$  were performed, and the storage modulus corresponding to the fundamental frequency during the oscillatory shear was measured. Typical storage modulus as a function of shear

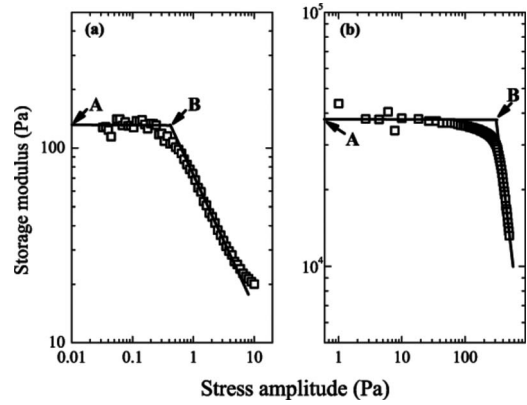


FIG. 6. Typical storage modulus as a function of shear stress amplitude for suspension (a) 40.4% and (b) 57.6%. Point A: plateau modulus. Point B: transition stress determined by the crossover of modulus plateau region and thinning region.

stress amplitude is shown in Fig. 6. Generally, the modulus are constant at low stress level, and  $G'$  is usually larger than  $G''$  even for the lowest concentration here. Storage modulus decreases first then increases with the increase in stress amplitude. The decrease of modulus is much sharper in highly concentrated suspensions, which is related to the rupture of certain structure and overcome of the yield stress. The plateau modulus at low stress and transition stress at the crossover of modulus plateau region and thinning region are obtained from Fig. 6. The plateau modulus and transition stress as function of concentration are shown in Figs. 7(a) and 7(b), respectively.

It is shown clearly in Fig. 7 that a sharp increase appears at almost the same concentration for different rheological properties. The value of critical concentration was obtained from a power law fit of  $y \propto (\phi - \phi_c)^{-n}$  to the data in Fig. 7, which gives  $\phi_c=49.5\% \pm 1.5\%$ . Similar transition has already been reported in some literatures but under different concentrations. A measured yield stress appears at lower volume fractions (above 50%) [28] for real spheres. For glass

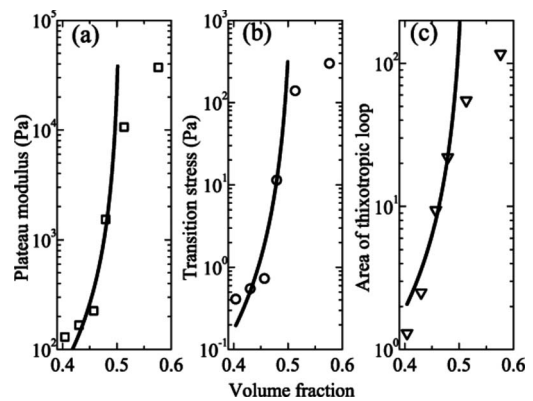


FIG. 7. Evolution of plateau modulus (a), transition stress (b) and loop area (c) with volume fraction. (a): plateau modulus determined by oscillatory stress sweep at the low amplitude. (b): transition stress obtained from the crossover of modulus plateau region and thinning region. (c): loop area of Fig. 5. Solid lines: power law fits of  $y \propto (\phi - \phi_c)^{-n}$ .

spheres in mineral oil, the critical packing fraction for jamming point was found at  $57.3\% \pm 1.3\%$  [29], which is smaller than the random close packing (RCP)  $\phi_{\text{rcp}}=64\%$  without friction or gravity. It is believed that the differences in the concentration of such transition can be ascribed to the polydispersity [3,30,31], particle friction, and difference of density [32,33] as well.

Actually, the critical concentration  $\phi_c$  is quite close to the “freezing” packing fraction ( $\phi_f \approx 0.49$  for three-dimensional spherical particles), which corresponds to a first order transition between hard-sphere solid and hard-sphere fluid [34]. The transition near  $\phi_c$  in colloidal suspensions with hard-sphere-like interactions has been show to be a first order transition from colloidal fluid to a crystallization [35]. The formation of crystals involves the creation of crystal nuclei containing a relatively large number of particles, and gives rise to the energetically unfavorable interface between crystal and liquid [36]. Fluid and crystal coexist between the freezing point  $\phi_f=0.494$  and the melting point  $\phi_m=0.545$  [34], while pure crystal is stable for  $\phi > \phi_m$ . Compared with crystallization in colloidal suspensions, noncolloidal suspensions with hard sphere show a critical volume fraction or freezing point at which the interparticle interactions should not be ignored and increase greatly with particle concentration and give rise to an evident yield stress. It is reasonable to regard this transition as “crystallization” since ordered behaviors have been shown via simulations using accelerated Stokesian dynamics for noncolloidal suspensions [11]. But we are unable to detect the possible ordered structures directly in our system at present. So, we avoid using the word crystallization and still call it critical volume fraction or freezing point, which corresponds to the definition of “dynamic jamming point” used by another author [29]. It is easy to understand that the above rheological results, i.e., significant increase in transition stress in oscillatory stress sweep and transient stress ramps, can also be regarded as a transition from fluidlike material to solidlike material.

Macroscopic properties of suspension are strongly associated with its internal microstructures, although it is very difficult to define the microstructure of suspensions experimentally by direct observation. However, the mean nearest neighbor surface distance between spherical particles can be estimated to guide the understanding on the microstructures. Figure 8 shows the concentration dependency of the upper bound of the dimensionless mean nearest neighbor surface distance,  $\tilde{d}=d/2R$  with  $R$  the mean radius of spherical particles, which is expressed as [37]

$$\frac{d}{2R} \leq \begin{cases} \frac{(1-\phi)^3}{24\phi(1-\phi/2)} & 0 < \phi \leq \phi_c \\ \frac{(\phi_m - \phi)}{24\phi g_f (\phi_m - \phi_c)} & \phi_c \leq \phi \leq \phi_m \end{cases}, \quad (1)$$

where  $g_f=(1-\phi_c/2)/(1-\phi_c)^3$  denotes the contact value of radial distribution function at the critical concentration  $\phi_c$ . The nearest neighbor particle distance generally decreases with the increase in the volume fraction, with a transition at  $\tilde{d}_c \approx 0.015$  for critical concentration  $\phi_c$ . If  $\tilde{d}_c$  is regarded as a

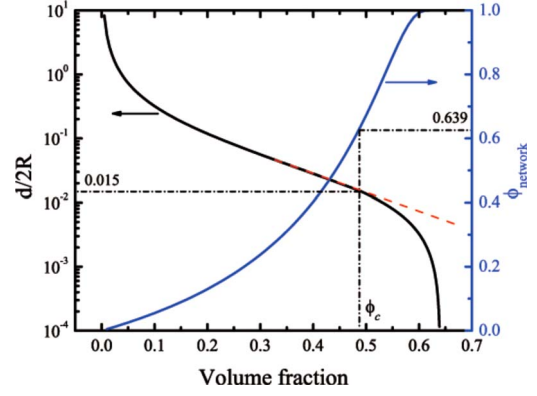


FIG. 8. (Color online) The upper bound of the dimensionless surface distance between particles and the fraction of network structure in the suspensions as a function of particle concentrations.

critical surface distance below which particles are believed to form a network, the mean fraction of particles  $\phi_{\text{network}}$  that take part in the formation of network structure can be estimated as

$$\phi_{\text{network}} = \int_1^{1+\tilde{d}_c} H(x) dx, \quad (2)$$

where the nearest neighbor distribution function  $H(x)$  is [35]

$$H(x) = 24\phi(a_0x^2 + a_1x + a_2)\exp\{-\phi[8a_0(x^3 - 1) + 12a_1(x^2 - 1) + 24a_2(x - 1)]\}, \quad (3)$$

with the coefficients

$$a_0 = \frac{1 + \phi + \phi^2 - \phi^3}{(1 - \phi)^3}, \quad a_1 = \frac{\phi(3\phi^2 - 4\phi - 3)}{2(1 - \phi)^3},$$

$$a_2 = \frac{\phi^2(2 - \phi)}{2(1 - \phi)^3} \quad \text{for } 0 \leq \phi \leq \phi_c \quad (4)$$

and

$$a_0 = 1 + 4\phi g_f \frac{\phi_m - \phi_c}{\phi_m - \phi},$$

$$a_1 = \frac{3\phi - 4}{2(1 - \phi)} + 2(1 - 3\phi)g_f \frac{\phi_m - \phi_c}{\phi_m - \phi},$$

$$a_2 = \frac{2 - \phi}{2(1 - \phi)} + (2\phi - 1)g_f \frac{\phi_m - \phi_c}{\phi_m - \phi}. \quad (5)$$

As shown in Fig. 8, the fraction of particles without interparticle attractions that form certain network in the suspension,  $\phi_{\text{network}}$ , increases with the particle concentrations. At the critical particle concentration  $\phi_c$ , about 63.9% ( $\approx 1 - e^{-1}$ ) particles in the suspension form a network structure that is defined by the critical surface distance  $\tilde{d}_c$ . This means that  $\phi_{\text{network}}$  can be used as a representation for the fluid-solid transition. Therefore, the critical volume fraction, or equivalently the freezing packing fraction, defines the transition from fluidlike to solidlike both from the changes in micro-

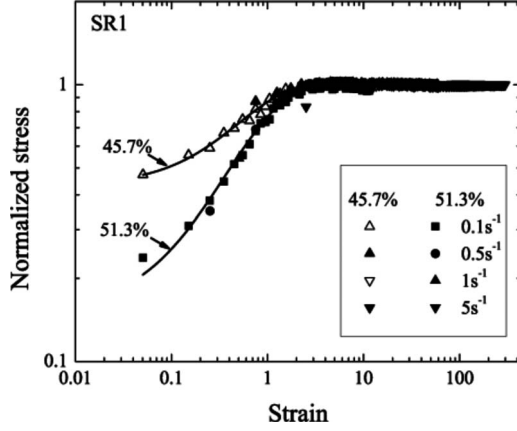


FIG. 9. Reduced stress vs strain for two suspensions (45.7% and 51.3%) in shear procedure SR1-A. The solid lines are the fitting curves with Eq. (6).

structures and rheological properties. However, this kind of structural or rheological transition is obtained from random distribution of particles without attractions and can serve as estimation on the network structures. The actual value should be somewhat different due to the attractions, particle size and size distribution and shape of frictional particles. However, we are unable to define clearly the dependence of  $\phi_{\text{network}}$  on any of these parameters at present. The liquid-to-solid transition can be different when the suspension is subjected to certain shear history, which will be shown in the following sections.

**B. Transient shear**

Suspension with four concentrations, 40.4%, 45.7%, 51.3%, and 56%, covering the critical concentration range, were used to study the rheological behaviors under complex shear history. Figure 8 shows a normalized transient stress as a function of shear strain ( $\gamma = |\dot{\gamma}|t$ ) after a step shear and rest (SR1-A). The stresses are normalized by the steady stress  $\tau_\infty$ . It is seen that the stress data under different shear rates ( $\dot{\gamma}_0 = \dot{\gamma}_a = 0.1, 0.5, 1, 5 \text{ s}^{-1}$ ) fall into a single curve for a specified suspension. This is consistent with the results for polystyrene particles suspended in silicone oil [3]. Such behavior is also predicted by the constitutive modeling of Phan-Thien and co-workers [30,38]. This approach models the motion of a generic pair of neighboring spheres in the suspension by a single pair of force-free and torque-free spheres tumbling along with the streamlines, and the interaction with the surrounding spheres is modeled by a diffusion-like process. This model predicts that the transient stress behavior can be reduced to a function of the applied strain. Preshear with other short shear histories (SR2 and SR3 in Fig. 2) show results similar to SR1 tests and are not shown here. The shear direction (in SR2) and the shear strength (in SR3) do not affect the normalized stress of suspensions with different concentrations.

Reduced curves in Fig. 9 evidently show the curve become shallower as the concentration decreases, and the transient stress responses behave concentration dependent under

TABLE I. Fitting parameters of the transient normalized stress by Eq. (4).

Concentration (vol%)	SSH (SR1-A)		LSH (SR3-A)	
	$a$	$\gamma_c$	$a$	$\gamma_c$
40.4	0.64	1.60	1.00	0.98
45.7	0.85	1.64	1.00	1.25
51.3	0.98	1.64	1.00	1.09
56	1.00	1.62	1.00	1.12

short shear history (SSH). If the concentration decreases further, the reduced stress curves will show even less strain dependence and the transient effect has almost disappeared [3]. The reduced stress curves in Fig. 9 can be described by the following model:

$$\tau(t)/\tau_\infty = 1 - a \exp(-\gamma/\gamma_c), \tag{6}$$

with  $a$  being the material parameter defined as  $(\tau_\infty - \tau_0)/\tau_\infty$ , which describe the contribution of the total change in filler distribution to the bulk stress, and  $\gamma_c$  as the characteristic strain. The fitted model parameters,  $a$  and  $\gamma_c$ , are listed in Table I. Under short shear history, the critical strain  $\gamma_c$  is similar for suspensions with different concentrations. However, the parameter  $a$  increases with concentration, and reaches a constant when the concentration is beyond the critical concentration  $\phi_c$  as shown in Table I. This agrees with the previous analysis on transition stress in oscillatory shear and transient stress ramps, where the samples are tested with short history of preshear or without preshear.

Figure 10 shows the reduced stress of two suspensions in SR2 of long shear history. It is found that the normalized stress decreases as the shear is repeated from SR2-A to SR2-C for relative dilute suspension (45.7%), while the normalized stress for relative concentrated suspension (51.3%) remains almost unchanged. For 51.3% suspension, the normalized stress in SR2-A is a little smaller than that of SR1-A, which denotes certain structural change by simple shear and reversed shear histories. After the complex sequential flow, the reduced stress curves of relative low concentration suspension (45.7%) get close to that of high concentration suspension (51.3%) and finally all curves mostly collapse into a single curve during the step SR2-C. Moreover, the test procedure SR3 in LSH is also performed to see the effect of shear rate ratio  $|\dot{\gamma}_a/\dot{\gamma}_0|$  on stress evolution of the suspensions. We continuously applied the test procedure SR3 with the ratio  $|\dot{\gamma}_a/\dot{\gamma}_0|$  of 0.5, 1, and 5, and the initial shear rate  $\dot{\gamma}_0$  of 0.1, 0.5, 1, and 5  $\text{s}^{-1}$ . Figure 11 shows the evolution of stress normalized by its steady value with strain for suspension 45.7%, 51.3% with shear rate ratio 0.5. The normalized stress curves collapse well into a single curve and show the particle concentration independence. The effect of ratio 1, 5 not shown here behave the similar tendency. This behavior is consistent with the reduced stress response of the step SR2-C.

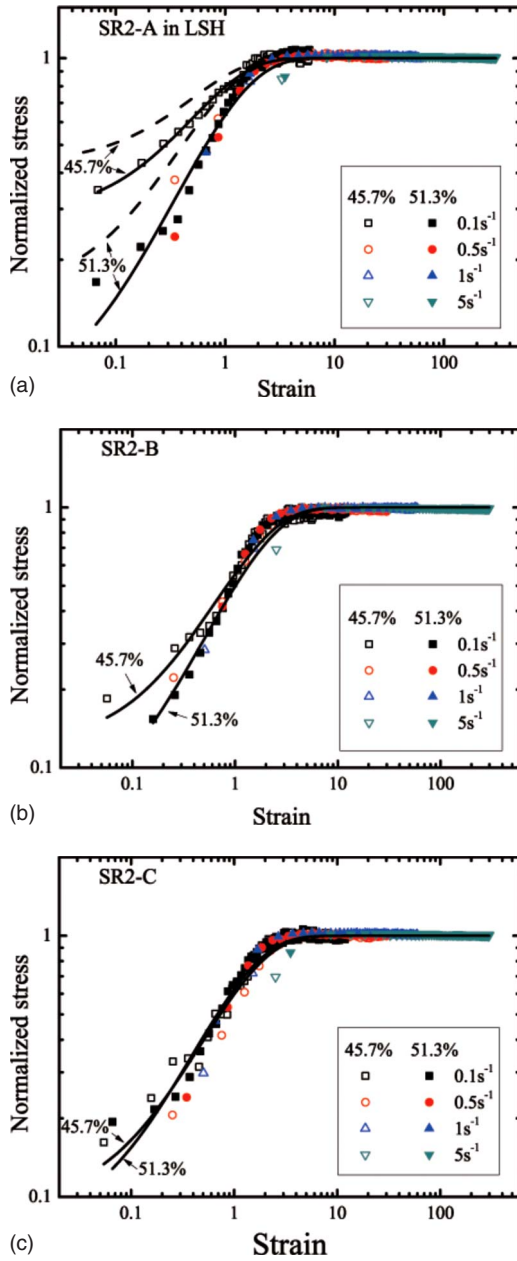


FIG. 10. (Color online) Reduced stress vs strain for two suspensions in different stages of SR2 in LSH. The solid lines represent the fitting curves by Eq. (6). The dash lines in (a) represent the fitting curves in SR1-A experiments with short shear history (SSH).

The transient stress responses show the concentration dependence under SSH, and concentration independence under LSH. A comparison of the normalized stress under different shear histories for suspensions with different concentrations is shown in Fig. 12. During the step SR1, different particle concentration results in different particle contribution to the shear stress. However, after long shear history, the normalized stress curves almost collapse into a single curve independent of particle concentration. However, the effect of preshear on suspensions with high concentration is more subtle, which cannot be seen from the reduced stresses. On the other hand, the characteristic strain  $\gamma_c$  is defined as the critical strain, at which the reduced stress reaches the value

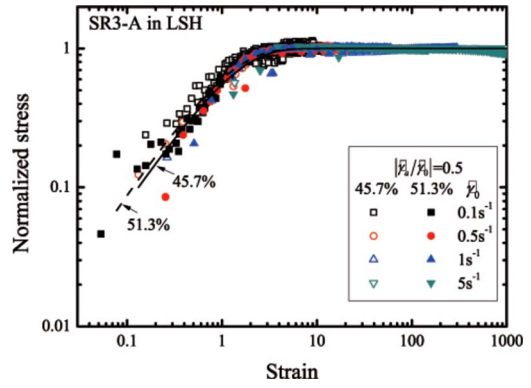


FIG. 11. (Color online) Reduced stress vs strain for suspensions of 45.7%, 51.3% during SR3-A with ratio 0.5. Solid line and dash line are the model fits explained in the text for 45.7% and 51.3%, respectively. The hollow symbols represent the 45.7% suspension, the solid symbols represent the 51.3% suspension. The squares, circles, up-triangles, and down-triangles stand for shear rate 0.1, 0.5, 1, and 5  $s^{-1}$ , respectively.

of  $\tau_\infty - (\tau_\infty - \tau_0)/e$ . It means that the critical strain is required to attain the certain suspension microstructure. The differences between the critical strain in SSH and LSH are probably caused by the shear-induced particle configuration. Although all suspensions display shear history dependent in SSH, the history dependence seems to limit to below  $\phi_c$ , bridge the gap between above and below  $\phi_c$  in LSH. Considering the solidlike behavior of suspension above  $\phi_c$ , the transition of the reduced stress from particle concentration dependent for  $\phi < \phi_c$  to concentration independent in LSH manifests a transition from the fluidlike behavior to the solidlike behavior for suspensions below  $\phi_c$ .

However, the structural change during the long time shear should be correlated with the change in rheological behavior especially for suspensions with concentration smaller than  $\phi_c$ . As discussed above, there is a liquid-solid transition after long shear history, it is assumed that the number of particle involved in the network structure increases and exceeds the critical network volume fraction ( $\phi_{network} \approx 0.49 \cdot 0.639 = 0.313$  for particles without attractions, see Fig. 8. This is just a speculation which needs further justification in future work. It is hard to say the exact  $\phi_{network}$  of attractive particles

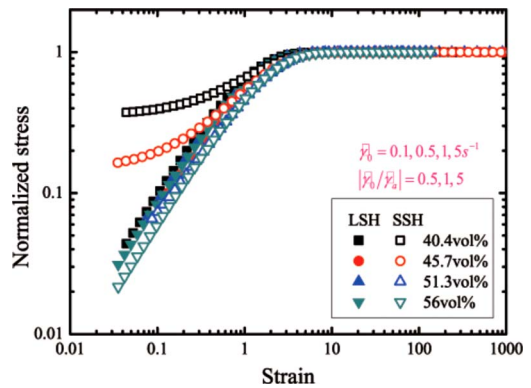


FIG. 12. (Color online) Fitting curves of the reduced stress under SSH (SR1-A) and LSH (SR3-A).

after long shear history). For a specific volume fraction ( $\phi < \phi_c$ ), shear flow can change the fraction of particles that forms network, i.e.,  $\phi_{\text{network}}$ . In a lot of phenomenological models of suspensions [39], the structural parameter  $\lambda$  is used to describe the degree of jamming. It has been shown above that  $\phi_{\text{network}}$  can be a function of shear history. This is expected to be important since the mechanical properties of suspensions are mainly contributed from  $\phi_{\text{network}}$ , and structural parameter in many phenomenological models can be related to the network fraction. However, such quantitative network parameter has not been considered by any previous phenomenological model. It is believed to be a good idea to incorporate the network volume fraction into phenomenological model, which might be very interesting when predicting the structures and rheology simultaneously.

### C. Nonlinear oscillatory shear

It has been shown above that transient shear history has the great effects on the structures of suspensions, which is manifested by the change in the reduced transient stress especially for suspensions with  $\phi < \phi_c$ . However, the transient shear is unable to show the effect of shear on concentrated suspensions with  $\phi > \phi_c$ . Besides the transient step shear, oscillatory shear could be an alternative to study the structure of suspensions since more information can be obtained such as the amplitude and nonlinearity of the responses signal. Compared with the transient experiments, the nonlinear oscillatory shear experiments was stress controlled since the input stress signal was easy to control and showed high S/N. An oscillatory stress sweep with increasing stress amplitude was applied to the suspensions, and the response signal of strain was recorded as a function of time. The nonlinear behavior in the response strain signal can be analyzed by the Fourier-transform rheology (FTR) method, although other interpretation can also be used [40]. The FTR used in oscillatory shear is a theoretically and experimentally simple method to describe time-dependent and nonlinear rheological phenomena. The mathematical procedures of Fourier-transform results in a power spectrum of frequency where only the fundamental and higher order harmonics appear. The most important higher order harmonics are odd ones, which are often related with structures of materials. Although even harmonics are observed sometimes, they are not well understood and will not be discussed here. Each peak of odd harmonics in power spectrum of strain is described by a magnitude  $\gamma_n$  and a phase  $\varphi_n$ . One way to quantify the degree of nonlinearity is the ratio of intensities ( $I_{n1} = \gamma_n / \gamma_1$ ) of the  $n^{\text{th}}$ -harmonic ( $\gamma_n$ ) to the first-harmonic ( $\gamma_1$ ). Alternatively, the complex compliance for the fundamental frequency and the third harmonic can be obtained, which is defined as

$$J^*(\omega, \tau) = \gamma(\omega, \tau) / \tau, \quad J_{3\text{rd}}^*(\omega, \tau) = \gamma_{3\text{rd}}(\omega, \tau) / \tau.$$

The first and third complex compliances of suspension are shown in Fig. 13. At low stress level, the complex compliance  $J^*$  is almost a constant and third complex compliances  $J_{3\text{rd}}^*$  in principle is negligible, which represents the yield behavior of suspensions. Since the instrumental noises could

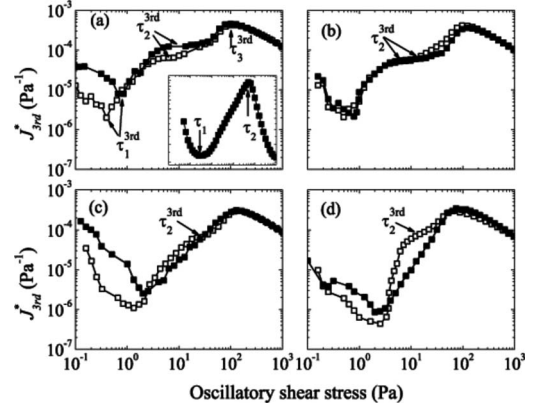


FIG. 13. Evolution of third-harmonic complex compliance with oscillatory shear stress for suspension 40.4% (a), 45.7% (b), 51.3% (c), 56% (d) with frequency of 1 Hz. Open square and line: without preshear. Solid square and line: after LSH. Inset in (a): determination of the critical stress by first complex compliance for 40.4%.

not be neglected at low stress, the third complex compliances in Fig. 13 show decreasing  $J_{3\text{rd}}^*$  from a finite value to the minimum compliance. As the stress amplitude increases, the complex compliance increases first, which represents the start of flow, and decreases later corresponding to the shear thickening behavior. The phase angle shows the similar behavior with the complex compliance. Two transition stresses shown in the first complex compliance,  $\tau_1$  and  $\tau_2$ , define the yield transition and the transition from shear thinning to shear thickening, respectively, see the inset of Fig. 13(a). However, there are three transitions shown by the minimum, shoulder and maximum of the third complex compliance, see Figs. 13(a)–13(d). Transition at  $\tau_1^{3\text{rd}}$  is consistent with  $\tau_1$ , which corresponds to the onset of nonlinear behavior at yielding. Moreover, there are two transition near  $\tau_2$ , i.e.,  $\tau_2^{3\text{rd}}$  and  $\tau_3^{3\text{rd}}$ .

In the transient experiments, the steady stress was used to normalize the transient stresses, and in the same way, the critical stress was selected to reduce the oscillatory stresses.  $\tau_1^{3\text{rd}}$  is taken as the critical stress to normalize the oscillatory stress. The oscillatory shear was applied after the suspensions were subjected to different shear history to show the effect of preshear on the microstructures. If there is a liquid-solid transition for low concentrations ( $\phi < \phi_c$ ) when subjected to shear history, the yield transition stress  $\tau_1^{3\text{rd}}$  determined by the oscillatory shear will increase with the shear history, as shown in Fig. 14 with measurement error of 0.15 Pa. Especially for suspensions with concentration smaller than  $\phi_c$ , the yield transition stress increases more obviously under long shear history, and becomes comparable with the transition stress at critical concentration, which denotes a liquid-solid transition.

Although several authors [3,8,10] have confirmed the relationship between large amplitude oscillatory shear (LAOS) rheology and the transient shear reversal rheology, LAOS experiments can provide more detailed and precise structural information than the transient experiments. Moreover, the stress-controlled LAOS experiments extend the range of strain amplitude. The strain used in the transient shear can be

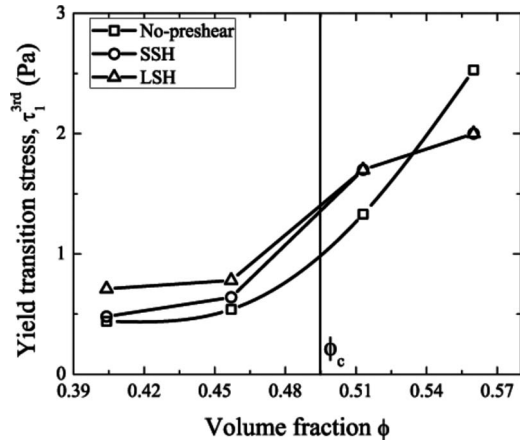
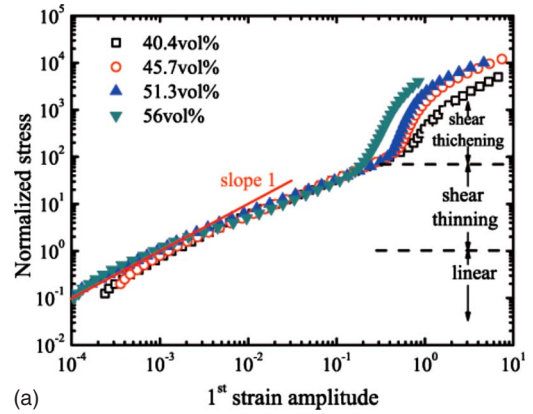


FIG. 14. The effects of shear history on the yield transition stress.

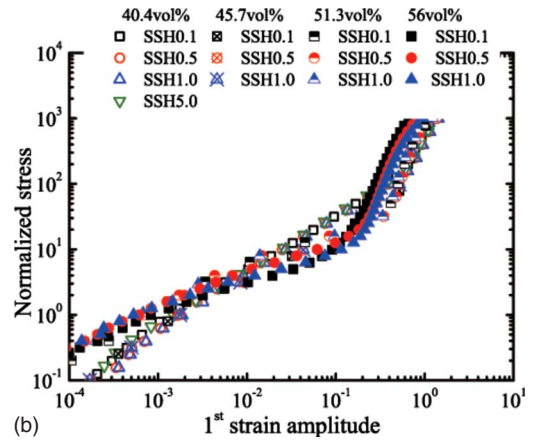
considered as macroscopic strain, as well as the strain of fundamental frequency in LAOS, corresponding to macroscopic deformation. However, the third-harmonic strain calculated from the harmonic distortions can be considered as a microscopic strain caused by suspension microstructure change. As discussed in the transient case, the evolution of the structure will be a function only of the imposed strain. Thus, the oscillatory stress normalized by the critical stress was plotted against the strain of the fundamental frequency and the third-harmonic strain, as shown in Figs. 15 and 16, respectively.

It is shown in Fig. 15 that the normalized oscillatory stress will increase linearly with the strain amplitude of first harmonic when normalized stress is smaller than 1, and the slope of log stress vs. log strain becomes smaller than 1 due to flow and shear thinning of suspensions. When the normalized stress increases further, the slope of stress and strain curve becomes much larger than 1 showing shear thickening behavior. The effects of preshear on the structures of suspensions can be seen from Fig. 15. Similar to the transient shear, the normalized oscillatory stress fall into a single curve independent of preshear rate. The difference in concentration is not evident in Fig. 15, although it has been shown in transient experiments that long shear history can make the liquidlike suspensions behave like a solid. Slight difference can be seen in the linear regime, where two groups of suspensions are separated by the critical concentration without preshear or under SSH, while the normalized stress under LSH for different concentrations are almost identical in the linear regime although the data is a little scattered. Therefore, the structures of suspensions are believed to be unaffected by the short preshear history greatly. The shear-thinning regime, corresponding to the structure destroys, does not exhibit difference for suspensions with different shear history.

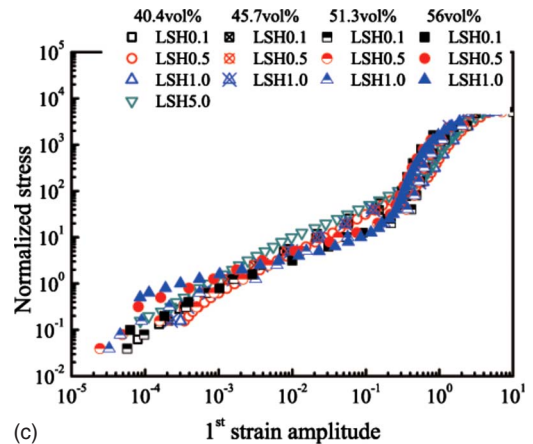
However, the reduced stresses show different responses with third-harmonic strain as shown in Fig. 16. It is seen from Fig. 16 that suspensions without preshear are divided into two groups according to the critical concentration  $\phi_c$ . Concentrated suspensions with  $\phi > \phi_c$  show stronger nonlinearity (large third-harmonic strain) than suspensions with  $\phi < \phi_c$ . When the suspensions are sheared with SSH, similar to



(a)



(b)



(c)

FIG. 15. (Color online) The normalized oscillatory stress as a function of the fundamental strain of suspensions with different preshear conditions: (a) No-preshear, (b) SSH, (c) LSH.

the transient experiments, suspensions display the concentration dependent stress responses and the normalized stresses as a function of third-harmonic strain are well separated for all the suspensions here. After the long shear history, suspensions are again separated into two types by the critical concentration  $\phi_c$ . Unlike the step shear or the fundamental strain in oscillatory shear, high harmonics in strain is more sensitive to the structure of network formed by particles. As an example, the effect of short shear history on suspensions with  $\phi > \phi_c$  can be well recognized, while their differences in step shear or in the normalized oscillatory vs first strain

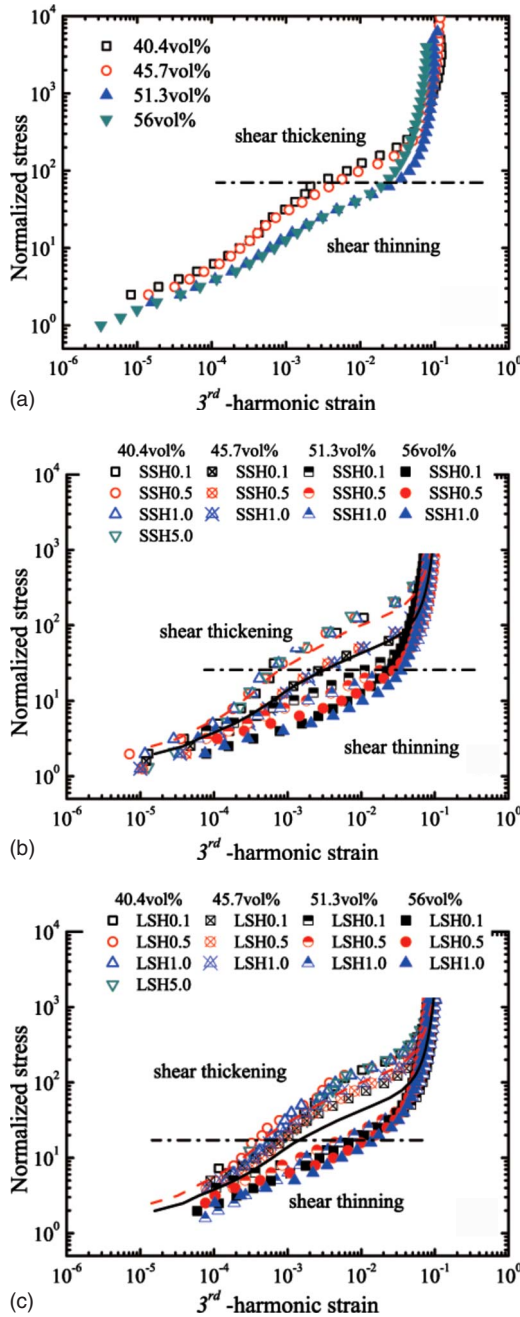


FIG. 16. (Color online) The normalized oscillatory stress as a function of the third harmonic strain of suspensions with different preshear conditions: (a) No-preshear, (b) SSH, (c) LSH. The dash and solid lines in (b) and (c) are suspensions of  $\phi < \phi_c$  and  $\phi > \phi_c$  without preshear, respectively.

amplitude are negligible. The other evident example is the third-harmonics for suspension with  $\phi < \phi_c$  after LSH is still different from that of  $\phi > \phi_c$ . This suggests a subtle difference in the structures formed by particles although the apparent reduced stress-strain curves become concentration independent after LSH. In another words, it is conjectured that the number of particles that take part in the network structure can increase due to LSH which cause an apparent liquid-solid transition for suspensions with  $\phi < \phi_c$ . However, the network characteristics are still different, which can be jus-

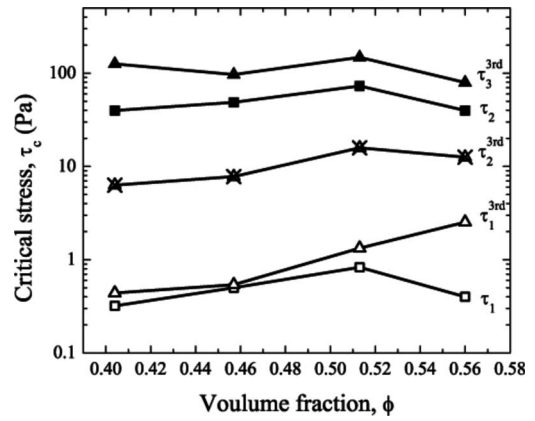


FIG. 17. Flow regions of suspensions without preshear. Square: critical stress determined by  $J^*$ ; Triangle: critical stress determined by  $J_{3rd}^*$ .

tified by the sensitivity of the structure to the increasing oscillatory stress, or the nonlinearity in the oscillatory shear.

**D. Interpretation of liquid-solid transition behavior: Shear effects on microstructure**

With the help of third-harmonic strain, it can be seen that suspensions with  $\phi < \phi_c$  and  $\phi > \phi_c$  exhibit different characteristics of the particle network, which are greatly affected by the shear history. To understand the stress behavior under LAOS flow, the corresponding microstructure should be studied. Briker and Butler [10,41] studied the correlation between stresses and microstructure in noncolloidal suspensions subject to oscillatory shear flow through experiments and simulations. Their experimental results show three different flow regimes in the curve of complex viscosity plotted as a function of applied strain amplitude, and the regimes were also confirmed by two-dimensional simulations. At low strain amplitude, an enhanced viscosity occurs corresponding to a microstructure with local ordering, where particles are partially trapped by their nearest neighbors. At intermediate strain amplitudes, a minimum in the viscosity occurs corresponding to an ordering of the suspension microstructure in the flow direction. At high strain amplitudes, the microstructure displays hydroclustering, and the rheology is similar with the steady shear rheology. Referring to their interpretations, the effects of shear history on the microstructural evolution of our systems under LAOS flow were investigated.

As a reference, the critical stresses of the suspensions without preshear were determined, see Fig. 17. The critical stresses  $\tau$  divide the diagram into three regimes [42] from the bottom up. For small stress amplitudes, there is a continuous network of interactions via direct contacts between particles, the particles are locked by their nearest neighbors and significant frictional interactions develop, and this defines the solidlike regime. For intermediate stress amplitudes larger than the yield stress, the continuous network of direct contacts is increasingly destroyed until the network disappears at sufficiently high stress, and then particles begin to order in the flow direction, this defines liquidlike regime. For larger stress amplitudes, the relative tangential motion of two close

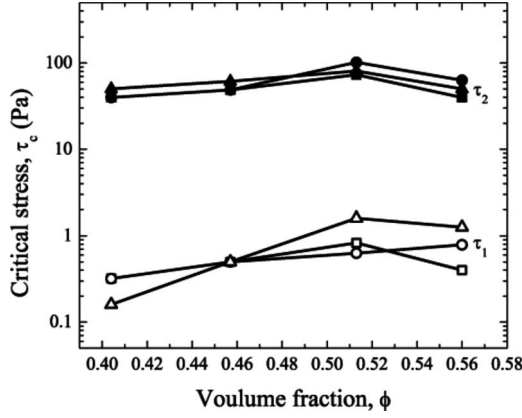


FIG. 18. The effects of shear history on the flow regions determined by  $\tau$ . Square: no-preshear; circle: SSH; triangle: LSH.

particles separated by a thin layer of fluid induces a normal force that tends to move the particles away from each other [12], which easily lead to flow-induced arching effects [28], this defines jamming/thickening regime. However, regions determined by critical stresses  $\tau^{3rd}$  differ from the regions by the critical stresses  $\tau$  in the middle flow region, where two additional regimes show up. The two additional regions may be related to the local behavior of suspensions in Couette flow. Through magnetic resonance imaging (MRI) technique, some authors [12–14] studied the local velocity and concentration profile of concentrated suspensions in Couette flow. It is well known that, in homogeneous shear flow, simple yield stress fluids should be approximately homogeneously sheared even at low shear rate values when the yield stress was overcome. However, MRI data [12–14] show the concentrated suspensions display severe heterogeneous velocity and concentration profile across the gap. Below the static yield stress, suspensions cannot flow and show solidlike behavior. Upon surpassing the yield stress, the flow localizes in a thin layer and cannot reach steady state. The thickness of this layer increases as the applied stress increases. At sufficiently high stress, the flow invades the entire sample and particles order in the flow direction and the flow reaches steady state within certain time scale. The process of invading displays an apparent shear-thinning behavior from macroscopic flow. After the entire flow, flow disturbance increases with the stress and leads to jamming at the certain stress level. Therefore, the regions determined by the critical stresses  $\tau^{3rd}$  show four regimes: solidlike, liquid-solid coexistence, liquidlike and jamming, from the bottom up.

Followed by a period of shear time shown in Figs. 2 and 3, the LAOS experiments were immediately performed. With increasing shear time, the critical stresses  $\tau$  as a function of concentration are plotted in Fig. 18. Except for the critical stress amplitudes of higher concentration is affected by increasing shear time, the flow regions determined by  $\tau$  are not influenced by shear history, still consist of three flow regimes. However, the flow regions determined by  $\tau^{3rd}$  of  $\phi > \phi_c$  are greatly affected by shear history. It can be seen from the Fig. 19, the dash square represents the second transition disappears when shear time increases for  $\phi > \phi_c$ . Under SSH or LSH, suspensions with  $\phi > \phi_c$  show larger third-

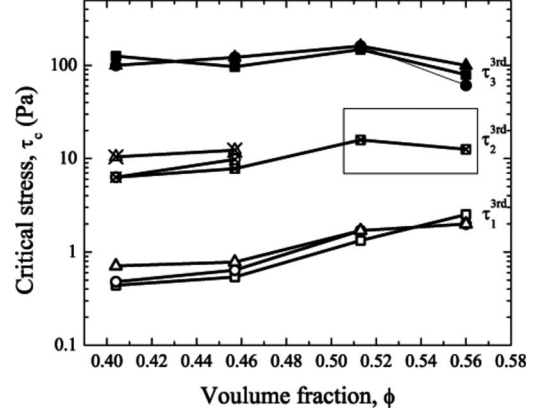


FIG. 19. The effects of shear history on the flow regions determined by  $\tau^{3rd}$ . Square: no-preshear; circle: SSH; triangle: LSH.

harmonic strain than  $\phi < \phi_c$ , which means that the shear history affects the microstructure of  $\phi > \phi_c$  much greater than  $\phi < \phi_c$ .

It is well known that one directional preshear is only designated to eliminate the influence of mechanical history and cannot homogenize the sample especially for concentrated suspensions, while oscillatory preshear or a series of shear reversals can uniform the suspensions. The two types of preshear make differences between the present transient shear and LAOS flow. In the transient step shear, the shear direction of data recording is opposite to that of former step shear, it means that the excess of particles is in the extensional quadrant instead of compressional quadrant when reversing the direction of flow [10]. However, under LAOS flow, the equilibrium position of oscillatory shear is consistent with the end of former step shear, it is reasonable to assume that the excess of particles in the extensional quadrant will affect the oscillatory behavior greatly compared with the step shear. In another word, step preshear before oscillatory flow will greatly heterogenize the suspensions with  $\phi > \phi_c$  than  $\phi < \phi_c$  so that the high concentrations cannot reach the overall shear state and directly from liquid-solid coexistence to flow jamming. This is also confirmed by the slope of normalized stress vs third-harmonic strain in Figs. 16(b) and 16(c). It can be seen that below the thickening stress, suspensions with  $\phi > \phi_c$  display the similar slope to the second transitional regime of  $\phi < \phi_c$ . Therefore, the liquid-like regime disappears when shear time increases for suspensions with  $\phi > \phi_c$ .

#### IV. CONCLUSIONS

In summary, based on the varying volume fraction, there is a solid-liquid transition with a critical volume fraction about  $49.5\% \pm 1.5\%$ . The transition behavior was confirmed through the critical transition stress measured by stress-shear rate curves, and shear history dependent LAOS behavior by FTR. Moreover, there is a preshear dependent liquid-solid transition, which is illustrated for suspensions with concentration below the critical volume fraction via transient step shear and LAOS after long shear history. Suspensions below  $\phi_c$  show the same reduced stress response as suspen-

sions above  $\phi_c$ , which suggests that the suspensions with lower concentration become apparent rigidity after long shear history. However, the microstructures or the local flow characteristics are still different for suspensions with concentration above and below  $\phi_c$  based on the FTR analysis. In

another words, even suspensions reach the same solidlike state and display the similar apparent rheological behaviors, microscopic or local flow behaviors could be different due to the differences in the microstructure or the characteristics of the particle packing.

- 
- [1] P. Gondret and L. Petit, *Phys. Fluids* **8**, 2284 (1996).  
 [2] C. Voltz, M. Nitschke, L. Heymann, and I. Rehberg, *Phys. Rev. E* **65**, 051402 (2002).  
 [3] F. Gadala-Maria and A. Acrivos, *J. Rheol.* **24**, 799 (1980).  
 [4] L. Heymann and N. Aksel, *Phys. Rev. E* **75**, 021505 (2007).  
 [5] L. Heymann, X. Chen, and N. Aksel, in *The XVth International Congress on Rheology*, The Society of Rheology 80th Annual Meeting, edited by A. Co *et al.* (American Institute of Physics, Monterey, California, 2008), p. 698.  
 [6] L. Heymann, S. Peukert, and N. Aksel, *Rheol. Acta* **41**, 307 (2002).  
 [7] V. G. Kolli, E. J. Pollauf, and F. Gadala-Maria, *J. Rheol.* **46**, 321 (2002).  
 [8] T. Narumi *et al.*, *J. Rheol.* **49**, 71 (2005).  
 [9] L. Heymann, S. Peukert, and N. Aksel, *J. Rheol.* **46**, 93 (2002).  
 [10] J. M. Bricker and J. E. Butler, *J. Rheol.* **51**, 735 (2007).  
 [11] A. Sierou and J. F. Brady, *J. Rheol.* **46**, 1031 (2002).  
 [12] P. Coussot, *Rheometry of Pastes, Suspensions, and Granular Materials* (Wiley, New York, 2005).  
 [13] N. Huang, G. Ovarlez, F. Bertrand, S. Rodts, P. Coussot, and D. Bonn, *Phys. Rev. Lett.* **94**, 028301 (2005).  
 [14] G. Ovarlez, F. Bertrand, and S. Rodts, *J. Rheol.* **50**, 259 (2006).  
 [15] J. A. Yosick *et al.*, *Rheol. Acta* **37**, 365 (1998).  
 [16] H. Komatsu, T. Mitsui, and S. Onogi, *J. Rheol.* **17**, 351 (1973).  
 [17] T. Matsumoto *et al.*, *J. Rheol.* **17**, 47 (1973).  
 [18] S. Onogi, T. Masuda, and T. Matsumoto, *J. Rheol.* **14**, 275 (1970).  
 [19] J. Dunwoody, *J. Non-Newtonian Fluid Mech.* **53**, 83 (1994).  
 [20] M. D. Graham, *J. Rheol.* **39**, 697 (1995).  
 [21] M. J. Reimers and J. M. Dealy, *J. Rheol.* **40**, 167 (1996).  
 [22] D. W. Adrian and A. J. Giacomin, *J. Rheol.* **36**, 1227 (1992).  
 [23] R. Mas and A. Magnin, *Rheol. Acta* **36**, 49 (1997).  
 [24] R. Pal, *Ind. Eng. Chem. Res.* **39**, 4933 (2000).  
 [25] J. G. Berryman, *Phys. Rev. A* **27**, 1053 (1983).  
 [26] T. Neidhöfer *et al.*, *Macromol. Rapid Commun.* **25**, 1921 (2004).  
 [27] J. Stickel and R. Powell, *Annu. Rev. Fluid Mech.* **37**, 129 (2005).  
 [28] C. Ancy, *Introduction to Fluid Rheology* (EPFL, Lausanne, 2005).  
 [29] E. Brown and H. M. Jaeger, *Phys. Rev. Lett.* **103**, 086001 (2009).  
 [30] I. E. Zarraga, D. A. Hill, and D. T. Leighton, *J. Rheol.* **44**, 185 (2000).  
 [31] P. T. Reardon *et al.*, *J. Phys. D* **41**, 115408 (2008).  
 [32] A. Fall, F. Bertrand, G. Ovarlez, and D. Bonn, *Phys. Rev. Lett.* **103**, 178301 (2009).  
 [33] K. J. Dong, R. Y. Yang, R. P. Zou, and A. B. Yu, *Phys. Rev. Lett.* **96**, 145505 (2006).  
 [34] W. Hoover and F. Ree, *J. Chem. Phys.* **49**, 3609 (1968).  
 [35] P. N. Pusey and W. van Meegen, *Nature (London)* **320**, 340 (1986).  
 [36] U. Gasser, *J. Phys.: Condens. Matter* **21**, 203101 (2009).  
 [37] S. Torquato, *Phys. Rev. E* **51**, 3170 (1995).  
 [38] T. Narumi *et al.*, *J. Rheol.* **46**, 295 (2002).  
 [39] P. Coussot, Q. D. Nguyen, H. T. Huynh, and D. Bonn, *Phys. Rev. Lett.* **88**, 175501 (2002).  
 [40] W. Yu, P. Wang, and C. Zhou, *J. Rheol.* **53**, 215 (2009).  
 [41] J. M. Bricker and J. E. Butler, *J. Rheol.* **50**, 711 (2006).  
 [42] I. Sumita and M. Manga, *Earth Planet. Sci. Lett.* **269**, 468 (2008).